Fast and Accurate Boundary Variation Method for Multi-layered Diffraction Optics

L. C. Wilcox[†], P. G. Dinesen[‡], and J. S. Hesthaven[†,*]

[†]*Division of Applied Mathematics, Brown University, Providence, RI 02912, USA*

[‡]*Kaleido Technology Aps, Ryttermarken 15, DK-3520 Farum, Denmark*

[1] A boundary variation method for the forward modeling of multi-layered diffraction optics is presented. The approach enables for fast and high-order accurate modeling of infinite periodic and finite aperiodic transmission optics, consisting of an arbitrary number of materials and interfaces of general shape, subject to plane wave illumination or, by solving a sequence of problems, illumination by beams The key elements of the algorithm are discussed as are details of an efficient implementation. Numerous comparisons with exact solutions and highly accurate direct solutions confirms the accuracy, versatility, and efficiency of the proposed method.

OCIS codes: 000.4430, 050.1970, 090.1970, 230.1950, 230.4170

1. Introduction

The ability to accurately and efficiently model multi-layered diffraction dominated optics has numerous applications, i.e., modeling of integrated transmission optics,

[1*] Corresponding author: Jan.Hesthaven@Brown.edu

Report Documentation Page

Form Approved
OMB No. 0704-0188

1. REPORT DATE	2. REPORT TYPE	3. DATES COVERED
2003		**00-00-2003 to 00-00-2003**

4. TITLE AND SUBTITLE	5a. CONTRACT NUMBER
Fast and Accurate Boundary Variation Method for Multi-Layered Diffraction Optics	5b. GRANT NUMBER
	5c. PROGRAM ELEMENT NUMBER
6. AUTHOR(S)	5d. PROJECT NUMBER
	5e. TASK NUMBER
	5f. WORK UNIT NUMBER
7. PERFORMING ORGANIZATION NAME(S) AND ADDRESS(ES) **Brown University,Division of Applied Mathematics,182 George Street,Providence,RI,02912**	8. PERFORMING ORGANIZATION REPORT NUMBER
9. SPONSORING/MONITORING AGENCY NAME(S) AND ADDRESS(ES)	10. SPONSOR/MONITOR'S ACRONYM(S)
	11. SPONSOR/MONITOR'S REPORT NUMBER(S)

12. DISTRIBUTION/AVAILABILITY STATEMENT
Approved for public release; distribution unlimited

13. SUPPLEMENTARY NOTES

14. ABSTRACT

15. SUBJECT TERMS

16. SECURITY CLASSIFICATION OF:			17. LIMITATION OF ABSTRACT	18. NUMBER OF PAGES	19a. NAME OF RESPONSIBLE PERSON
a. REPORT **unclassified**	b. ABSTRACT **unclassified**	c. THIS PAGE **unclassified**		**39**	

design and analysis of Bragg mirrors, and integrated cavities. Such methods would also enable the modeling of random variations in design due to manufacturing limitations, as well as serve as fast forward solvers in inversion as part of an quality control process.

For binary periodic structures, the rigorous coupled-wave analysis has been widely used to model such optical elements during the last decade.[9] However, the need to analyze structures with aperiodic non-binary features of finite extent and bean illumination requires that alternatives be sought. This has lead to the development of several alternative approaches, e.g., Finite-Element,[14] Boundary element,[12] Finite-Difference Time-Domain,[16] and Spectral Collocation.[8,10,11] The latter two methods both compute a direct solution of the time-domain vectorial Maxwell equations and are very general in being adaptable to a wide variety of geometries and physical settings. As the need to model problems of realistic size and complexity becomes more pressing, however, the memory and computational time requirements of such direct volume methods quickly becomes a limiting factor not only for the design process but also for the analyses of particular structures.

In this work we take a different approach, building on the boundary variation method proposed in.[3,4,5] These methods are founded on the observation that solutions to electromagnetic diffraction by a periodic structure depend analytically on a variation of the interface. In other words, diffraction from a smooth grating can be determined from knowledge of reflection and refraction at a plane interface. Using this result, fast and accurate high-order perturbation schemes for finite-size perturbations have been developed for modeling of two- and three-dimensional metallic and trans-

mission gratings[3,4,5] illuminated by plane waves. These methods were subsequently extended to include problems illuminated by guided waves[6,7] and verified extensively by comparisons with direct high-order solution of Maxwell equations.

We continue the development of these methods by demonstrating the use of the boundary variation methods in an iterative approach to accurately and efficiently model multi-layered optics, e.g., transmission optics where it is essential to accurately account for the internal reflections. To make this feasible, we discuss in some detail the implementation which relies on properties of the scattering process to make it efficient. The proposed algorithm is shown to perform well for period and nonperiodic problems and results agrees very well with directly computed reference solutions, albeit obtained a dramatically reduced computational cost.

What remains of this paper is organized as follows. In Sec. 2 we discuss the basic setup and the essential details of the formulation. This sets the stage for Sec. 3 where we introduce the boundary variation method, first for a single interface and subsequently for the general multiple interface problem. Key elements of an efficient implementation is also discussed here. In Sec. 4 we offer a number of test cases to illustrate the efficiency and capability of the proposed approach, while Sec. 5 concludes with a few remarks and outlines future work.

2. Problem Setup and Model

As illustrated in Fig. 1 we consider a two-dimensional situation in which a monochromatic plane wave

$$\begin{bmatrix} \boldsymbol{E}^{\rm inc}(\boldsymbol{x},t) \\ \\ \boldsymbol{H}^{\rm inc}(\boldsymbol{x},t) \end{bmatrix} = \begin{bmatrix} \boldsymbol{A}_E \\ \\ \boldsymbol{A}_H \end{bmatrix} \exp\Big[i(\boldsymbol{k}^{\rm inc}\cdot\boldsymbol{x}-\omega t)\Big] \quad ,$$

propagating in the homogeneous region, Ω^0, impinges on a structure of multi-layered non-magnetic homogeneous regions $\Omega^1,\ldots,\Omega^N$, separated by the smooth periodic interfaces, $\Gamma^1,\ldots,\Gamma^N$, described by the functions, $f^1(x),\ldots,f^N(x)$ For each region Ω^j we have the associated permittivities, ε^j. Furthermore, we have introduced the complex amplitudes, $\boldsymbol{A}_E$ and $\boldsymbol{A}_H$, for the electric and magnetic field, respectively, while $\boldsymbol{k}^{\rm inc}$ signifies the wavevector of the incoming field, restricted to propagate in the (x,y)-plane, i.e., $\boldsymbol{k}^{\rm inc}=(k_x^{\rm inc},k_y^{\rm inc})$. Recall that

$$\boldsymbol{k}^{\rm inc}=\frac{2\pi}{\lambda_v}\sqrt{\varepsilon^0}\hat{\boldsymbol{k}}^{\rm inc} \quad , \quad \omega=2\pi\frac{c_v}{\lambda_v} \quad .$$

Without loss of generality we can normalize length and time such that the vacuum wavelength, $\lambda_v=1$, and the vacuum speed of light is $c_v=1$.

The illumination of the structure generates the fields $(\boldsymbol{E}^j,\boldsymbol{H}^j)$ in the region Ω^j for all $j\in\{0,1,\ldots.N\}$. Clearly, these fields satisfy the time-harmonic Maxwell equations

$$\nabla\times\boldsymbol{E}^j=i\omega\boldsymbol{H}^j \quad , \quad \nabla\times\boldsymbol{H}^j=-i\omega\varepsilon^j\boldsymbol{E}^j \quad , \quad \forall j\in\{0,1,\ldots.N\} \quad ,$$

under the constraint that the fields are solenoidal, i.e.,

$$\nabla\cdot\boldsymbol{E}^j=\nabla\cdot\boldsymbol{H}^j=0 \ \ \forall j\in\{0,1,\ldots.N\} \quad .$$

In Ω^0, the total field is given as $(\boldsymbol{E}^{\text{inc}}, \boldsymbol{H}^{\text{inc}}) + (\boldsymbol{E}^0, \boldsymbol{H}^0)$, i.e., in this case $(\boldsymbol{E}^j, \boldsymbol{H}^j)$ represents the scattered field while $(\boldsymbol{E}^j, \boldsymbol{H}^j)$ signifies the total fields otherwise.

The fields in the homogeneous regions, Ω^{j-1}, and Ω^j are connected through the boundary conditions along Γ^j for all $j \in \{1, \ldots, N\}$. In particular, along the interface Γ^j, endowed with an outward pointing normal vector, $\hat{\boldsymbol{n}}^j$, separating the two dielectric regions Ω^{j-1} and Ω^j, continuity of the tangential field components requires

$$\hat{\boldsymbol{n}}^j \times \begin{bmatrix} \boldsymbol{E}^{j-1} + \delta_{j-1,0}\boldsymbol{E}^{\text{inc}} \\ \\ \boldsymbol{H}^{j-1} + \delta_{j-1,0}\boldsymbol{H}^{\text{inc}} \end{bmatrix} = \hat{\boldsymbol{n}}^j \times \begin{bmatrix} \boldsymbol{E}^j \\ \\ \boldsymbol{H}^j \end{bmatrix} \quad .$$

In the special case where Γ^j is assumed to be a perfect conductor, this condition degenerates to a Dirichlet condition on the electric field as

$$\hat{\boldsymbol{n}}^j \times \boldsymbol{E}^{j-1} = -\hat{\boldsymbol{n}}^j \times \delta_{j-1,0}\boldsymbol{E}^{\text{inc}} \quad .$$

When solving Maxwell's equation it is often advantageous to express the boundary condition on $\boldsymbol{H}^j$ through the condition on $\boldsymbol{E}^j$ and Maxwell's equations themselves as a Neumann condition

$$\begin{aligned} \hat{\boldsymbol{n}}^j \times \nabla \times \left(\boldsymbol{H}^{j-1} + \delta_{j-1,0}\boldsymbol{H}^{\text{inc}}\right) &= -\hat{\boldsymbol{n}}^j \cdot \nabla \left(\boldsymbol{H}^{j-1} + \delta_{j-1,0}\boldsymbol{H}^{\text{inc}}\right) \\ &= -\frac{\partial(\boldsymbol{H}^{j-1} + \delta_{j-1,0}\boldsymbol{H}^{\text{inc}})}{\partial \hat{\boldsymbol{n}}^j} = 0 \quad , \end{aligned}$$

along the perfectly conducting interface Γ^j.

To simplify matters further, we restrict ourselves to problems where Ω^j can be considered homogeneous and where the incoming fields are two-dimensional and either TE or TM polarized. This implies that the local solutions to the scattering/penetration problems satisfies the homogeneous Helmholtz equation

$$j = 0, \ldots, N \;\; : \;\; \Delta u^j + |k^j|^2 u^j = 0 \quad , \tag{1}$$

where $u^j = E_z^j$ in the case of TE-polarized illumination and $u^j = H_z^j$ for a TM-polarized incoming wave. Furthermore, $|k^j| = 2\pi\sqrt{\varepsilon^j}$ represents the magnitude of the local wavevector under the normalization discussed in the above.

This system of Helmholtz equations, Eq.(1), must be solved subject to the conditions that

$$u^{j-1}(x, f^j(x)) - u^j(x, f^j(x)) = -\delta_{j-1,0} u^{\mathrm{inc}}(x, f^j(x)) \ , \tag{2}$$

and

$$\begin{aligned} \frac{\partial}{\partial \hat{\boldsymbol{n}}^j} u^{j-1}(x, f^j(x)) \quad - \quad & C_j \frac{\partial}{\partial \hat{\boldsymbol{n}}^j} u^j(x, f^j(x)) \\ & = -\frac{\partial}{\partial \hat{\boldsymbol{n}}^j} \delta_{j-1,0} u^{\mathrm{inc}}(x, f^j(x)) \ , \end{aligned} \tag{3}$$

at a general di-electric interface. The constant C_j takes the values

$$C_j = \begin{cases} 1 & \text{TE Polarization} \\ \varepsilon^{j-1}/\varepsilon^j & \text{TM Polarization} \end{cases} .$$

In the case where Γ^j represents a perfectly conducting object the conditions are different for the two polarizations, i.e., we have a Dirichlet condition in case of a TE-polarized wave

$$u^{j-1}(x, f^j(x)) = -\delta_{j-1,0} E_z^{\mathrm{inc}}(x, f^j(x)) \ ,$$

while we recover a Neumann condition on the tangential magnetic field as

$$\frac{\partial}{\partial \hat{\boldsymbol{n}}_j} u^{j-1}(x, f^j(x)) = -\frac{\partial}{\partial \hat{\boldsymbol{n}}_j} \delta_{j-1,0} H_z^{\mathrm{inc}}(x, f^j(x)) \ ,$$

along the metallic interface in case the illuminating wave is TM-polarized.

To complete the specification of the problem we require that the solutions, u^0 and u^N, are bounded at infinity and that solutions consists of purely outgoing waves. The means by which we enforce these conditions are closely related to the computational approach chosen to solve the above system of coupled Helmholtz equations.

3. Boundary Variation Method

As we solve the general multiple interface problem as a sequence of single interface problems we first discuss the single interface scheme in detail and subsequently consider the extension to the general case.

A. Single interface scheme

Let us assume that we only have a single interface, Γ, separating the two homogeneous regions, $\Omega^+ = \Omega^0$ and $\Omega^- = \Omega^1$, illuminated by a two-dimensional TE or TM polarized wave. We take the amplitude of the illuminating TE or TM wave is 1.

The interface, Γ, is assumed to be L-periodic along x, and described by $f(x)$. Since the incident wave is a plane wave, the fields, $u^{\pm}(\boldsymbol{x})$, are endowed with a similar periodicity, i.e.,

$$u^{\pm}(x+L,y) = \exp(ik_x^{\rm inc}L)u^{\pm}(x,y) \quad .$$

Following,[15] we shall fix the notation by introducing

$$K = \frac{2\pi}{L} \quad , \alpha_n = k_x^{\rm inc} + nK \quad , \alpha_n^2 + (\beta_n^{\pm})^2 = |k^{\pm}|^2 \quad ,$$

where K simply reflects the wavenumber associated with the periodicity, α_n represents the Bragg condition for lattice refraction/reflection while the last condition expresses energy conservation. In accordance with the orientation of the problem, see Fig. 1, we

shall use the notation that $\beta_n^{\pm} \leq 0$ as the incoming wave propagates in the negative y-direction. Also, to ensure boundedness of waves at infinity, we have that $\mathrm{Im}(\beta_n^{\pm}) \leq 0$ for the evanescent waves. Clearly there can only be a finite number of propagating modes since for n being sufficiently large, $\beta_n^{\pm}$ becomes purely imaginary.

Away from the interface, Γ, we now express the solution, $u^{\pm}(x,y)$, as a Rayleigh expansion

$$u^{\pm}(x,y) = \sum_{n=-\infty}^{\infty} B_n^{\pm} \exp\left[i(\alpha_n x \mp \beta_n^{\pm} y)\right] \quad .$$

Conservation of energy implies that

$$\sum_{n\in\Pi^+} \beta_n^+ \left|B_n^+\right|^2 + C_0 \sum_{n\in\Pi^-} \beta_n^- \left|B_n^-\right|^2 = k_y^{\mathrm{inc}} \quad ,$$

where $\Pi^{\pm}$ represent the subset of $\beta_n^{\pm}$ corresponding to the propagating waves, i.e., $\beta_n^{\pm} \leq 0$ is real. For purely metallic scattering the second part of the sum drops out.

In this setting, the unknowns are the Rayleigh coefficients, $B_n^{\pm}$, which depends on the profile, $f(x,d,\theta)$. Following,[3] we introduce a new profile

$$f_\delta(x) = \delta f(x,L) \quad ,$$

i.e., $\delta = 0$ corresponds to a flat horizontal interface, while $\delta = 1$ represents the original profile.

The heart of the boundary variation method introduced in[3,4] is the assumption that the Rayleigh coefficients, $B_n^{\pm}(\delta)$, can be expressed as a Taylor series in δ,

$$B_n^{\pm}(\delta) = \sum_{k=0}^{\infty} \frac{1}{k!} \frac{d^k B_n^{\pm}(0)}{d\delta^k} \delta^k = \sum_{k=0}^{\infty} d_{k,n} \delta^k \quad ,$$

i.e., we assume that $B_n^{\pm}$, and hence $u^{\pm}$, are analytic in the boundary variation, δ.

The validity of this is by no means obvious but has nevertheless been established rigorously in.[2]

To sketch the way by which one can obtain $d_{k,n}$, let us consider the simplest case in which Ω^- is a perfectly conducting metallic object illuminated by a TE-polarized plane wave, i.e., the boundary condition is

$$u^+(x, f_\delta(x)) = -\exp\left[ik_x^{\rm inc}x + ik_y^{\rm inc}\delta f(x)\right] \quad .$$

¿From the Rayleigh expansion itself we have

$$\left.\frac{1}{k!}\frac{\partial^k u^+}{\partial\delta^k}\right|_{\delta=0} = \sum_{n=-\infty}^{\infty} d_{k,n}\exp\left[i(\alpha_n x - \beta_n^+ y)\right] \quad . \tag{4}$$

We can, however, also evaluate the variation of u^+ with respect to δ at $y = 0$ using the boundary condition as

$$\begin{aligned}\left.\frac{1}{r!}\frac{\partial^r u^+}{\partial\delta^r}\right|_{y,\delta=0} &= -(ik_y^i)^r\frac{f^r}{r!}\exp(ik_x^{\rm inc}x) \\ &- \sum_{k=0}^{r-1}\frac{f^{r-k}}{(r-k)!}\frac{\partial^{r-k}}{\partial y^{r-k}}\left[\frac{1}{k!}\frac{\partial^k u^+}{\partial\delta^k}\right]_{y,\delta=0} \quad .\end{aligned} \tag{5}$$

Let us introduce the Fourier expansion of the periodic interface, $f(x, L)$, as well as powers of it as

$$\frac{f(x,L)^r}{r!} = \sum_{l=-rF}^{rF} C_{r,l}\exp(iKlx) \quad . \tag{6}$$

Using Eq.(4) to evaluate the y-derivative of $1/k!\partial^k u^+/\partial\delta^k$ we can, by combining Eqs.(4)-(6), recover an explicit forward recurrence for the unknown expansion coefficients, $d_{k,n}$, of the Rayleigh coefficients on the form

$$\begin{aligned}d_{k,n} = \quad & -(ik_y^{\rm inc})^k C_{k,n} + \\ & \sum_{r=0}^{k-1}\sum_{q=\max[-rF,n-(k-r)F]}^{\min[rF,n+(k-r)F]} C_{k-r,n-q}(-i\beta_q)^{k-r}d_{r,q} \quad .\end{aligned}$$

Hence, given all expansion coefficients, $d_{s,t}$, and $C_{s,t}$, $s < k$, $-sF \leq t \leq sF$, we can recover all expansion coefficients for $s = k$ by forward recurrence.

Albeit of a more complicated form, similar recurrences can be derived for TM-polarized illumination[3] as well as for TE and TM polarized illumination of a general di-electric interface.[4] Recurrences for illumination by guided waves can be found in.[6,7]

While this yields an approach for computing the Taylor expansion of the Rayleigh coefficients

$$B_n(\delta) = \sum_{k=0}^{K} d_{k,n}\delta^k \quad ,$$

it is generally not an easy matter to evaluate this expansion outside its circle of convergence. To partially overcome this we express the Taylor series by its Padé-approximation as

$$B_n(\delta) = \frac{a_0 + a_1\delta + ... + a_L\delta^L}{1 + b_1\delta + ... + b_M\delta^M} \quad ,$$

where the coefficients are found by standard means by requiring that it be equivalent to the Taylor series for $D = M + L + 1$. In subsequent discussions we shall take $M = L = D/2$. As it is well known, Padé-approximations have remarkably better convergence properties than Taylor series[1] and suffices for the present investigation.

With this in place, we can compute the Rayleigh coefficients of the global solution, $u^{\pm}(x, y)$, at different angles of incidence, controlled by $\boldsymbol{k}^{\text{inc}}$, using only knowledge of the Fourier representation of the interface, Γ.

B. Multiple interface scheme

Exploiting the linearity of the Helmholtz equation and considering a geometrical optics series, the single interface scheme will be used repeatedly to form the scheme

for multiple interfaces. The approximate solution for the single interface case is given as a plane wave expansion

$$u^{\pm}(x,y) = \sum_{n=-p}^{q} B_n^{\pm} \exp\left[i(\alpha_n x \mp \beta_n^{\pm} y)\right] \quad . \tag{7}$$

where $n \in \{-p, \ldots, q\}$ is the set of waves for which $\beta_n^{\pm} \leq 0$ is real. The non-propagating waves are disregarded in the single interface case as we focus on modeling of the far field. For other applications requiring detailed near-field information, these evanescent waves could be included.

In the multiple interface scheme the solution for the first interface, Γ^1, is computed first. This is a sum of plane waves, Eq.(7), propagating away from the interface. The waves traveling away from the multi-layer structure are not propagated any further. However, the waves traveling down into the multi-layer structure are propagated to the next interface by updating the phase by the phase factor $\exp(i\beta d)$. Here d is the vertical distance between the interfaces. The single interface boundary variation method is subsequently used on each of these propagated waves at the new interface. As this process continues, a set of plane waves in each region is computed, the sum of which gives the approximate solution in that region.

By conservation of energy there must be a finite number of directions in which the waves can travel within each region, i.e., the multiple interface scheme only evokes the single interface scheme a finite number of times. When the multiple interface algorithm starts, the single interface scheme is called a finite number of times for a wave of unit amplitude in all the possible wave directions to build an efficiency table. When the single interface scheme is needed a lookup in the efficiency table based on

the direction of the incident wave and the region it lives in produces the efficiencies and directions of the refracted and reflected waves. The amplitudes of the refracted and reflected waves are found by multiplying the efficiencies by the amplitude of the incident wave. Using the fact that there is a finite number of possible waves the method can group waves to limit the computations. The following section will make this need apparent in order to make the approach computationally efficient.

C. Implementation

Let us first consider the example of a double interface structure, Fig. 2. The structure has a top interface, Γ^1, which gives rise to three diffractive plane waves when illuminated. The second interface, Γ^2, is taken to be planar for simplicity. With the incident plane wave, $\boldsymbol{E}^{\text{inc}}(\boldsymbol{x}, t)$, and the top interface, Γ^1, the single interface boundary variation method is used to compute the solution

$$\boldsymbol{E}^{\pm}(x, y) = \sum_{n=-1}^{1} \boldsymbol{E}_n^{\pm} \quad ,$$

where

$$\boldsymbol{E}_n^{\pm} = B_n^{\pm} \exp\left[i(\alpha_n x \mp \beta_n^{\pm} y)\right] \quad \forall n \in \{-1, 0, 1\} \quad .$$

We assume that the boundary variation method emits a solution which is the summation of three plane waves for the region Ω^0 and three plane waves for the region Ω^1. To track the solutions the implementation employs a solution set, S^n, associated with each region, Ω^n. These are initialized to the empty set for $n \in \{0, 1, 2\}$. The solutions are added to their respective sets $S^0 = S^0 \cup \{\boldsymbol{E}_n^+\}_{n=-1}^1$ and $S^1 = S^1 \cup \{\boldsymbol{E}_n^-\}_{n=-1}^1$. The plane waves, $\{\boldsymbol{E}_n^+\}_{n=-1}^1$, travel away from the interface and requires no further

consideration prior to evaluating the far field. The remaining waves $\{\boldsymbol{E}_n^-\}_{n=-1}^1$ are traveling towards Γ^2 and we propagate these waves by simply updating the phase. For the wave, $\exp(i\beta_{-1}^- d)\boldsymbol{E}_{-1}^-$, we need to solve the single interface problem at Γ^2. However, as Γ^2 is a flat plane we use the Fresnel's equations to compute the reflected and refracted waves exactly, $\boldsymbol{E}_{-1,0}^{-+}$ and $\boldsymbol{E}_{-1,0}^{--}$, respectfully. The waves are added to the solution sets so $S^1 = S^1 \cup \{\boldsymbol{E}_{-1,0}^{-+}\}$ and $S^2 = S^2 \cup \{\boldsymbol{E}_{-1,0}^{--}\}$. The wave $\boldsymbol{E}_{-1,0}^{--}$ is propagating in the negative y direction away from the optical element and need not be considered further. However, $\boldsymbol{E}_{-1,0}^{-+}$ is traveling towards Γ^1 and eventually interacts with Γ^1 from below, i.e., the interaction is computed using the single interface algorithm with the $-f^1(x)$ profile. This process of collecting the solution waves from the single interface boundary condition and propagating the waves in Ω^1 to accounted to multiple internal reflections is continued as long as needed.

For the general multi-layer problem with N interfaces, we initialize our method with the region Ω^0 and the incident wave $\boldsymbol{E}^{\text{inc}}$ by adding $(\boldsymbol{E}^{\text{inc}}, \Omega^0, T^{\text{ttl}})$ to the wave set W^0. Here T^{ttl} signify time-to-live as a measure of how the maximum number of internal reflections a wave and its children can undergo. All of the solution sets are initialized to the empty set, $S^n = \{\emptyset\}$. Also let $D^l = \sum_{j=0}^{l} d^j$ where d^j is the thickness of the layer Ω^j. With this notation, we must choose $d^0 = d^N = 0$.

To initialize the efficiency table we first note that in any given layer the local Bragg condition is $\alpha = k_x^{\text{inc}} + \sum_{j=1}^{N} |k^j|^2 m_j$ where m_j is an integer for $j = 1, 2, \ldots, N$. Also for each region Ω^j we have conservation of energy

$$\alpha^2 + \beta^2 = |k^j|^2 \quad .$$

Recall that we only consider the waves for which β is real, i.e. there are a finite number of waves in each layer and we can find all possible directions a wave will be traveling in each layer using the Bragg conditions.

The single interface boundary variation code can be run for incident waves of unit magnitude for each of these possible directions in each layer and the resulting efficiencies are stored in a separate hash table for each layer. The key to the hash table is the direction of the incident wave. In the case of an incident wave illumination a flat plane interface the computations are simplified by using Fresnel's equations[17] instead of the single interface boundary variation code.

Assume now that we are considering a wave that has undergone m bounces and is scheduled undergo the next bounce. First note that $\boldsymbol{E} = A\exp\left[i(\alpha x + C\beta y)\right]$, where $C = -1$ if the wave is traveling in the positive y direction and $C = 1$ if the wave is traveling in the negative y direction. For an element $w = (\boldsymbol{E}, \Omega^l, T^{\text{ttl}})$ from the set of active waves, W^n, this wave is propagated by updating the phase through multiplication by $\exp(i\beta d^l)$ and using the single interface method at the particular interface with the initial wave $\boldsymbol{E}\exp(i\beta d^l)$. This yields the solution

$$u^{\pm}(x,y) = \sum_{n=-p}^{q} \boldsymbol{E}_n^{\pm} \ ,$$

where

$$\boldsymbol{E}_n^{\pm} = B_n^{\pm}\exp\left[i(\alpha_n x \mp \beta_n^{\pm} y)\right] \quad \forall n \in \{-p, -p+1, \ldots, q\} \ .$$

Each wave is added to a set corresponding to each layer, i.e., $S^l = S^l \cup \{\exp(-C\beta D^{\max\{l,l+C\}})\boldsymbol{E}_n^{+}\}_{n=-p}^{q}$ and $S^{l+C} = S^{l+C} \cup \{\exp(-C\beta D^{\max\{l,l+C\}})\boldsymbol{E}_n^{-}\}_{n=-p}^{q}$.

Next we determine if we should add the newly computed waves to the set W^{m+1}

of active waves. If the $T^{\text{ttl}} - 1 = 0$ then the waves *time to live* is up and it is not propagated further, i.e., no waves are added to the set. Alternatively, if a particular amplitude is below a given threshold, w_ϵ, we can decide not to propagate this wave any further.

Furthermore, if $l + C \in \{1, 2, \ldots, N\}$ then the waves $(\{\boldsymbol{E}_n^-\}_{n=-p}^q, \Omega^-, T^{\text{ttl}} - 1)$ are added to the set W^{m+1}. If $C \neq 1 \vee l \neq 0$ then the waves $(\{\boldsymbol{E}_n^+\}_{n=-p}^q, \Omega^+, T^{\text{ttl}} - 1)$ are added to the set W^{m+1}. When waves are added to the set W^{m+1} it is first checked if a wave with the same direction and region is already in W^{m+1}. If so then the amplitude of the wave is added to the amplitude of the wave already in the set. If there is no wave with the same direction in the same region then the wave is simply added to W^{m+1}. Due to the conservation of energy, there are only a maximum of M waves independent of m in W^{m+1}. Without this accounting for multiple waves at similar direction of propagation, the number of active waves would grow exponentially, rendering the computational work prohibitive.

The end of going from bounce m to $m + 1$ is reached when all the waves are in W^m. To get the approximate multi-layer solution in the region Ω^l we sum up the elements in S^l.

It is possible to use the L_2 difference in solutions of different T^{ttl}'s at a few given y-values near the interfaces to evaluate the convergence as a measure of accuracy. In each region, Ω^j, there is a solution set S^j which holds a finite number of waves, e.g., s^j. We consider the error, ϵ, in energy by the relation for the scattering efficiencies

$$\epsilon = \sum_{l=1}^{s^0} e_l^0 + \frac{\varepsilon^0}{\varepsilon^N} \sum_{l=1}^{s^N} e_l^N - 1 \ , \tag{8}$$

where $e_l^j = \beta_l^j |B_l^j|^2/\beta^{\text{inc}}$ is the efficiency and $B_l^j \exp\left[i(\alpha_l^j x + C_l^j \beta_l^j y)\right]$ is a wave in S^j. Note that S^0 does not include the incident wave and $C_l^j = -1, 1$ denotes the direction in which the wave is traveling.

It is worth while emphasizing that a small energy deficiency, ϵ, does *not* imply convergence to the correct solution but simply checks self consistency.

4. Verification and Convergence

In the following we shall attempt to validate the accuracy and general performance of the proposed scheme for several different multi-layer two-dimensional optical elements. When available, we shall compare with exact solutions. However, for more interesting cases, these are not available and we compare against independently verified highly accurate solutions obtained with a spectral multi domain time-domain code.[8,10]

A. Plane interfaces

In the case where all interfaces are planar the solution is known on analytic form[17] as

$$u^j = A_1^j \exp\left[i(\alpha_1^j x - \beta_1^j y)\right] + A_2^j \exp\left[i(\alpha_2^j x + \beta_2^j y)\right] \quad ,$$

within each layer, assuming that the stack of layers is illuminated by a plane wave, $A\exp\left[i(\alpha x - \beta y)\right]$. The unknown amplitudes are found by connecting the solutions through the boundary conditions Eqs.(2,3) with $A_1^0 = A_2^N = 0$. For the wave directions we have $\alpha_1^j = \alpha_2^j = \alpha$, $|\alpha| + |\beta_1^j| = |k^{j+1}|$ and $|\alpha| + |\beta_2^j| = |k^j|$. This forms a linear system which can be solved producing A_l^j for $j = 0, \ldots, N$ and $l = 1, 2$. We can then compare the amplitude of the solution given by the exact solution, $|A_l^j|$, with the

amplitude of the solution given by the multi-layer boundary variation scheme, $|B_l^j|$, for $j = 0, \ldots, N$ and $l = 1, 2$ as a function of bounces.

1. Thin plate

For the first test we consider a normal TE wave of unit amplitude illuminating a thin plate (see Fig. 3). We use Fresnel's equations to solve the single interface problems and take the wave amplitude threshold of $w_\epsilon = 10^{-15}$, i.e., all waves are allowed to live for a maximum number of bounces.

In Fig. 3 we see that the solution, or rather the amplitudes, converges exponentially fast in the number of bounces to the exact solution. The importance of accounting for the internal reflections is evident even for this simple test case.

When comparing the solutions we look at the error in complex amplitude of the waves in the exact solution A_l^j with the computed solution B_l^j. As we increase the number of bounces, i.e., Tttl beyond 22 the error remains constant. This is because the wave amplitude threshold w_ϵ is now fully responsible for terminative the the waves.

2. Thin plate stack

A further test of accuracy is illustrated in Fig. 4, reflecting a normal TE wave of unit amplitude illuminating four thin plates stacked on top of each other. Again we use Fresnel's equations to solve the single interface problems since all of the interfaces are planar and choose the wave threshold to be $w_\epsilon = 10^{-15}$.

This problem provides a test of the collecting of waves being propagated into the set W^{m+1} into a finite number of waves independent of number of bounces m. The work to compute the solution increases linearly with the number of bounces because

of this collection process.

As is clear from Fig. 4 there is exponentially fast convergence to the exact solution as the number of internal reflections increases. We can compute down to machine precision with 90 bounces in less than two tenths of a second on an average desktop computer. For bounces greater than 90 the wave tolerance w_ϵ determines when the waves stop propagating

B. Single curved interfaces

In the following we provide a few tests in which one interface is curved while all other remain planar. For simplicity, and supported by the general verifications in the above, we just consider the two-interface case. All results are compared to fully converged results obtained with a high-order accurate full field solver.[8,10]

1. Shallow single curve

This problem consists of a normal TE wave of unit amplitude illuminating a thin plate with one sinusoidal interface and a flat bottom as illustrated in Fig. 5. The single interface interactions with the sinusoidal interface, Γ^1, are calculated using a [31/31] Padé approximant. The interactions with Γ^2 are calculated using Fresnel's equations.

The wavelength-to-period ratio of Γ^1 is small, 0.16, providing a simple test of the multi-layer boundary variation code. While building the efficiency table, the single interface boundary variation scheme is used 8 times to compute possible wave interactions with Γ^1 and the maximum error in the energy efficiency for the single interface

cases is 1.33×10^{-15}.

In Table 1 we increased the number of allowed internal bounces sufficiently to ensure that the wave tolerance, w_ϵ, is the factor that controls when the waves stop propagating. This table shows that the energy conservation from the single interface scheme is kept as the number of bounces increase, i.e., there does not appear to be severe problems of error accumulation.

To check the overall accuracy of the scheme, we illustrate in Fig. 6 and Fig. 7 the solutions obtained from the multi-layer code with results in a different manner. We see in Fig. 6 the importance of considering the multiple internal reflections. In Fig. 7 we have increased the number of internal reflections to ensure that waves are propagated until their amplitude is below $w_\epsilon = 10^{-15}$, yielding excellent agreement with the reference solution.

As one could expect, the multi layered boundary variation approximation becomes more accurate as the distance from the structure increases. This is a consequence of not including the evanescent waves which remain in the reference solution. The excellent agreement of the fields at different values of y confirms that the phases of the fields are correct to a similar level of accuracy. This is confirmed by direct comparisons which we omit for briefness.

2. Deeper single curve

To further test the algorithm, we consider a the case of a TE polarized wave illuminating a two-interface problem in which the top interface is varies considerably more than in the above case, see Fig. 8. In this case the wavelength-to-period ratio of Γ^1

is 0.5. The single interface interactions with Γ^1 are calculated using a [49/49] Padé approximant, leading to a maximum error in the efficiency for the single interface cases of $\mathcal{O}(10^{-7})$.

As the number of internal reflections increased to ensure that it does not restrict the propagation of the waves, the energy conservation is $\mathcal{O}(10^{-6})$. Thus, as in the above simpler case, we find that the energy conservation of the multi-layer boundary variation scheme is largely controlled on the maximum error in the efficiency for the single interface cases.

In Fig. 9 we have increased the bounces large enough so that all waves are propagated until the amplitude is below $w_\epsilon = 10^{-15}$. The agreement with the reference solution is excellent and improves as one moves away from the structure.

C. Lens

As an example of a more general nonperiodic problem, we consider a Gaussian lens being illuminated by a normal TE wave of unit amplitude. The setup is illustrated in Fig. 10. Here $f^1(x) = 0.5\exp(-x^2)$ for $x \in (-7.5, 7.5]$ and periodically extended. The periodicity of Γ^1 is set large enough so that its effect on the solution is small, thus approximating a non-periodic surface. For the Fourier transform of Γ^1, needed by the single interface boundary variation scheme, we use 33 modes, and the solutions are calculated using a $[37, 37]$ Padé approximant. Since Γ^2 is flat, Fresnel's equations are used to calculate the scattering and penetration.

The multi-layer boundary variation solution in Fig. 11 is for a sufficiently high number of internal reflections to ensure convergence, i.e., is given for the amplitude is

less than $w_\epsilon = 10^{-15}$. In this case the error in efficiency is 0.8. However, the comparison with the direct solution reveals excellent agreement, in particular away from the lens.

D. Double curved interfaces

As a final test to illustrate the versatility of the developed scheme, we consider a TE wave of unit amplitude illuminating a thin structure with two curved interfaces, illustrated in Fig. 12. In this case, both Γ^1 and Γ^2 are sinusoidal and a [49/49] Padé approximant is used to calculate the single interface interactions. The number of internal reflections is sufficiently high to ensure that all waves are propagated until their amplitude is below $w_\epsilon = 10^{-15}$

The results, shown in Fig. 12, show excellent agreement between the multi-layer boundary variation scheme and the directly computed reference solution. The only exception is $y = -0.5$. This can be attributed to the strong evanescent waves produced by the two curved interfaces and the high contrast. Here the error in efficiency is $\mathcal{O}(10^{-13})$.

5. Concluding Remarks

The main purpose of this work has been to develop an efficient and accurate computational approach to model multi layered optical elements, possibly with nonperiodic profiles and arbitrary profiles at each interface separating layers of homogeneous nonmagnetic magnetic materials.

At the heart of the scheme is a very efficient boundary variation method for accurately solving the problem of reflection and refraction by a single interface, be

it material or metallic. The methods exploits the linearity of Helmholtz equation along with the Bragg condition to significantly reduce the amount of space and time needed to compute the solutions, consisting of numerous internally reflected waves. A detailed understanding of the scattering processes allows us to collect the waves into a finite set of active waves, limiting the otherwise exponentially growing set of waves. Following a setup phase, tens-of-thousands of internally reflected waves can subsequently be computed a very little additional cost.

In the cases presented here the evanescent waves produced by the single interface boundary variation scheme are disregarded as we have focused on the solution away from the grating structure. However, for other applications, one could include these in a way similar to that used for propagating waves. Given that the kernel is the single interface scheme, the limitations is set by this, i.e., in double precision arithmetic, the depth-to-wavelength ratio of the variations of the interfaces can not exceed $\mathcal{O}(1)$. Using extended precision can help on this although the cost typically increases also.

To check the accuracy of the multi-layer boundary variation code it has been extensively validated through direct comparisons with high-order accurate time-domain solutions, showing excellent agreement, at a dramatically reduced cost as compared to the direct solution.

While these results offer the first step in the development of a general high-order accurate method for the efficient modeling of multi-layer diffractive optics, a number of important issues remain open. Straightforward extensions include illumination by Gaussian beams, by solving a sequence of problems subject to plane wave illumination, and the use of the threshold w_ϵ to adaptively control the work and requested accu-

racy. Extensions to the three-dimensional vectorial case is likewise straightforward, following the developments in.[5,7] This sets the stage for the use of such methods as efficient and accurate forward solvers in an optimal design loop, as demonstrated for the simplest metallic case in.[13] We hope to pursue such developments in the near future.

Acknowledgment

The work of the first author (LCW) was supported by an NSF sponsored VIGRE program at Brown University. The work of the last author (JSH) was partially supported by ARO under contract DAAD19-01-1-0631, by NSF through an NSF Career Award, and by the Alfred P. Sloan Foundation through a Sloan Research Fellowship.

References

1. G. A. Baker and P. Graves-Morris, *Padé Approximants*, 2nd Edition. Encyclopedia of Mathematics and its Applications **59** (Cambridge University Press, Cambridge, UK., 1996).
2. O. Bruno and F. Reitich, *Solution of a boundary value problem for Helmholtz equation via variation of the boundary into the complex domain*, Proc. R. Soc. Edin. A **122**(1992), pp. 317–340.
3. O. Bruno and F. Reitich, *Numerical Solution of Diffraction Problems: A Method of Variation of Boundaries*, J. Opt. Soc. Am. A **10**(1993), pp. 1168–1175.
4. O. Bruno and F. Reitich, *Numerical Solution of Diffraction Problems: A Method of Variation of Boundaries. II. Finitely Conducting Gratings, Padé Ap-*

proximants, and Singularities, J. Opt. Soc. Am. A **10**(1993), pp. 2307–2316.

5. O. Bruno and F. Reitich, *Numerical Solution of Diffraction Problems: A Method of Variation of Boundaries. III. Doubly Periodic Gratings*, J. Opt. Soc. Am. A **10**(1993), pp. 2551-2562.
6. P. G. Dinesen and J. S. Hesthaven, *A Fast and Accurate Boundary Variation Method for Diffractive Gratings*, J. Opt. Soc. Am. A **17**(2000), pp. 1565-1572.
7. P. G. Dinesen and J. S. Hesthaven, *A Fast and Accurate Boundary Variation Method for Diffractive Gratings. II. The Three-Dimensional Vectorial Case*, J. Opt. Soc. Am. A **18**(2001), pp. 2876-2885.
8. P. G. Dinesen, J. S. Hesthaven, J. P. Lynov, and L. Lading, *Pseudospectral Method for the Analysis of Diffractive Optical Elements*, J. Opt. Soc. Am. A **16**(1999), pp. 1124-1130.
9. T. K. Gaylord and M. G. Moharam, *Analysis and applications of optical diffraction by gratings*, Proc. IEEE **73**(1985), pp. 894–937.
10. J. S. Hesthaven, P. G. Dinesen, and J. P. Lynov, *Spectral Collocation Time-Domain Modeling of Diffractive Optical Elements*, J. Comput. Phys. **155**(1999), pp. 287-306.
11. J. S. Hesthaven, *High-Order Accurate Methods in Time-Domain Computational Electromagnetics: A Review*, Adv. Imag. Elec. Phys. **127**(2003) – to appear.
12. K. Hirayama, E. N. Glytsis, T. K. Gaylord, and D. W. Wilson, *Rigorous electromagnetic analysis of diffractive cylindrical lenses*, J. Opt. Soc. Am.

A, **13**(1996), pp. 2219–2231.

13. K. Ito and F. Reitich, A High-Order Perturbation Approach to Profile Reconstruction: I. Perfectly Conducting Gratings, Inverse Problems **15**(1999), pp. 1067–1085.

14. B. Lichtenberg and N. C. Gallagher, *Numerical modeling of diffractive devices using the finite element method*, Opt. Eng. **33**(1994), pp. 1592–1598.

15. R. Petit, *A tutorial introduction*, in Electromagnetic Theory of Gratings, R. Petit, ed., **22** of Topics in Current Physics (Springer-Verlag, Berlin, 1980), pp. 1–52.

16. D. W. Prather and S. Shi, *Formulation and application of the finite-difference time-domain method for the analysis of axially symmetric diffractive optical elements*, J. Opt. Soc. Am. A, **16**(1999), pp. 1131–1141.

17. P. Yeh, *Optical Waves in Layered Media*, (John Wiley & Sons, New York, 1988).

List of Figure Captions

Fig. 1 Generic setup for scattering by a problem with multiple interfaces.

Fig. 2 Specific example to illustrate scheme for a problem with two interfaces.

Fig. 3 On the left is shown the problem setup for the test with one plane layer while the right shows the decay of error in field amplitudes as a function of internal reflections or bounces.

Fig. 4 On the left is shown the problem setup for the test with a stack of plane layers while the right shows the decay of error in field amplitudes as a function of internal reflections or bounces.

Fig. 5 Problem specification for a single layer with a shallow curved interface.

Fig. 6 E_z computed at different heights, y, with $y = 0$ corresponding to the vertical position of the shallow curved interface. Illumination is TE-polarized at normal incidence. Results are shown for a fixed number of internal bounces, and compared to a highly accurate spectral solution, illustrating the importance of accounting for the multiple internal reflections.

Fig. 7 E_z computed at different heights, y, with $y = 0$ corresponding to the vertical position of the shallow curved interface. Illumination is TE-polarized at normal incidence. Results are shown for converged solutions in terms of internal reflections and compared to a highly accurate spectral solution.

Fig. 8 Problem specification for a single layer with a deep curved interface.

Fig. 9 E_z computed at different heights, y, with $y = 0$ corresponding to the vertical position of the deep curved interface. Illumination is TE-polarized at normal inci-

dence. Results are shown for converged solutions in terms of internal reflections and compared to a highly accurate spectral solution.

Fig. 10 Problem specification for a single layer with an integrated lens.

Fig. 11 E_z computed at different heights, y, with $y = 0$ corresponding to the vertical position of the integrated lens. Illumination is TE-polarized at normal incidence. Results are shown for converged solutions in terms of internal reflections and compared to a highly accurate spectral solution.

Fig. 12 Problem specification for a single layer with two curved interfaces.

Fig. 13 E_z computed at different heights, y, with $y = 0$ corresponding to the vertical position of the slowly varying interface. Illumination is TE-polarized at normal incidence. Results are shown for converged solutions in terms of internal reflections and compared to a highly accurate spectral solution.

List of Table Captions

Table. 1 Convergence of scattering efficiencies and relation to threshold value, w_ϵ, used in iterative approach.

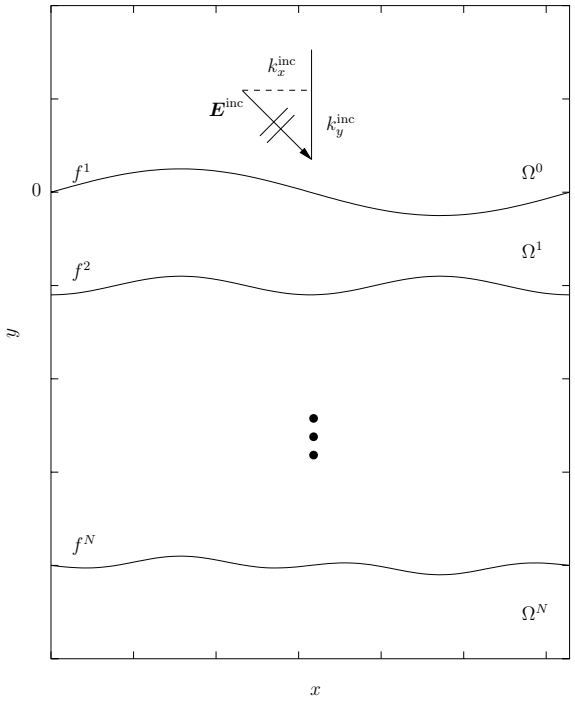

Fig. 1. Generic setup for scattering by a problem with multiple interfaces.

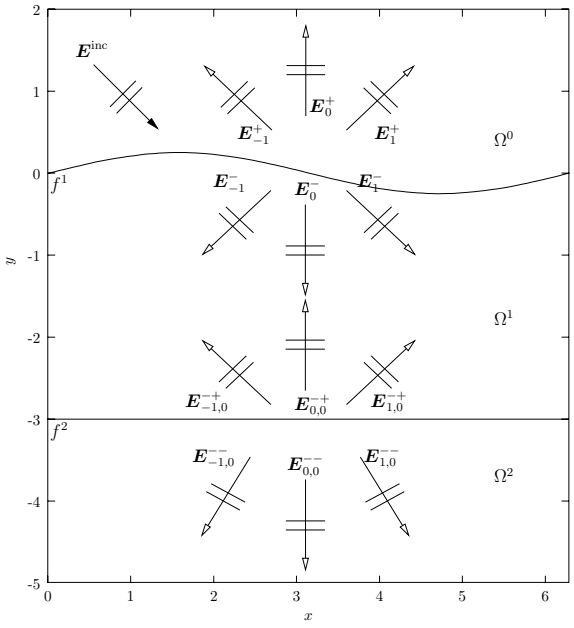

Fig. 2. Specific example to illustrate scheme for a problem with two interfaces.

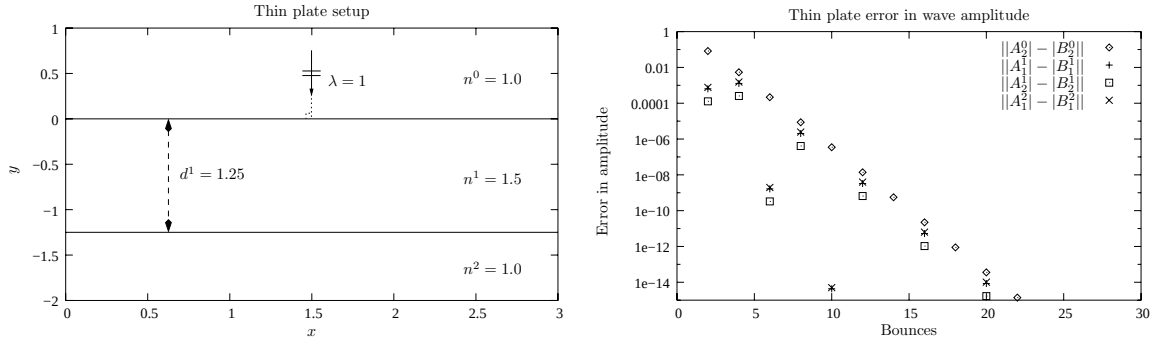

Fig. 3. On the left is shown the problem setup for the test with one plane layer while the right shows the decay of error in field amplitudes as a function of internal reflections or bounces.

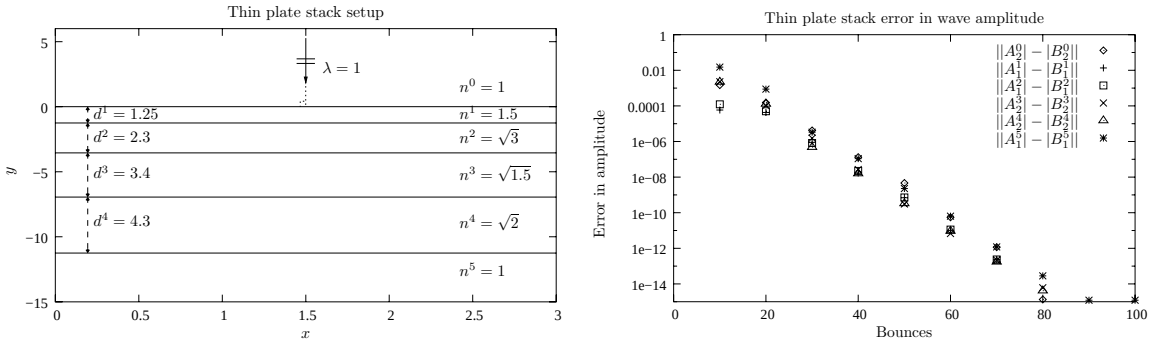

Fig. 4. On the left is shown the problem setup for the test with a stack of plane layers while the right shows the decay of error in field amplitudes as a function of internal reflections or bounces.

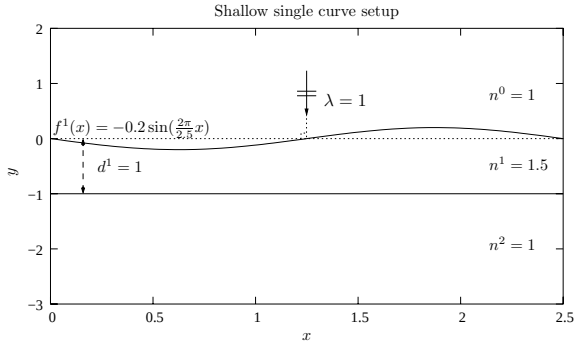

Fig. 5. Problem specification for a single layer with a shallow curved interface.

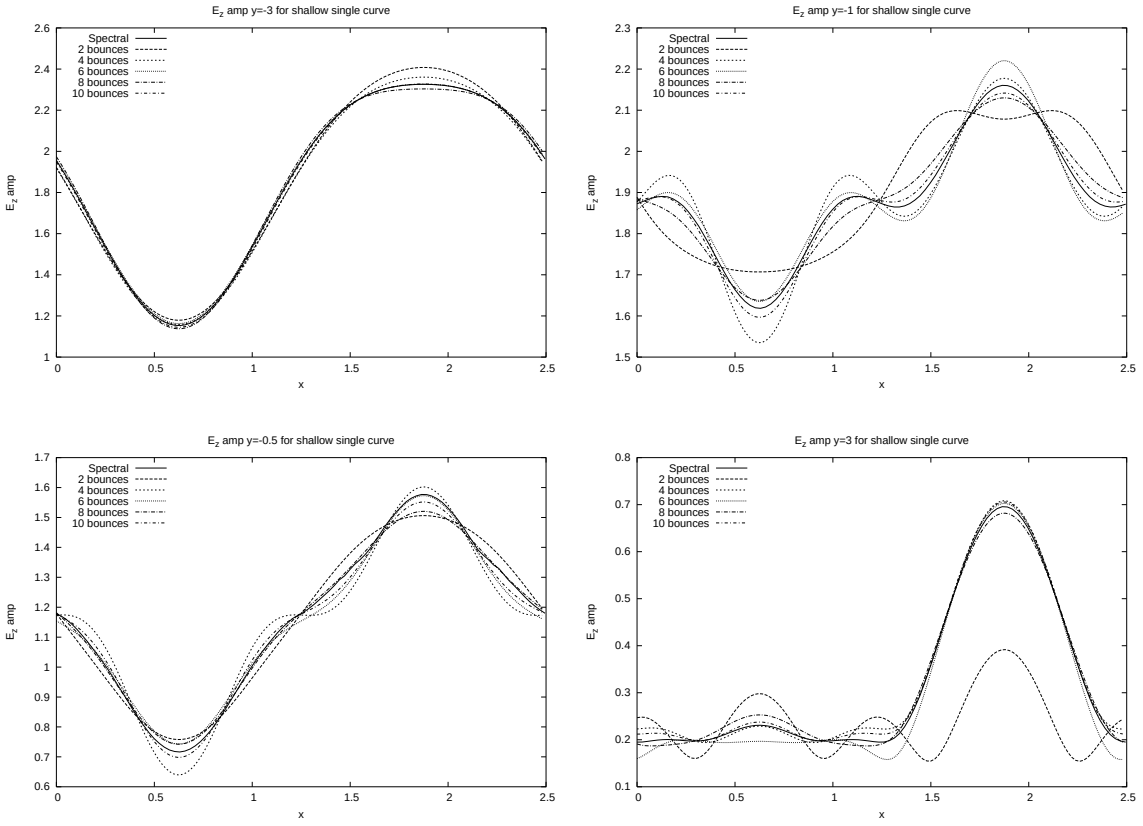

Fig. 6. E_z computed at different heights, y, with $y = 0$ corresponding to the vertical position of the shallow curved interface. Illumination is TE-polarized at normal incidence. Results are shown for a fixed number of internal bounces, and compared to a highly accurate spectral solution, illustrating the importance of accounting for the multiple internal reflections.

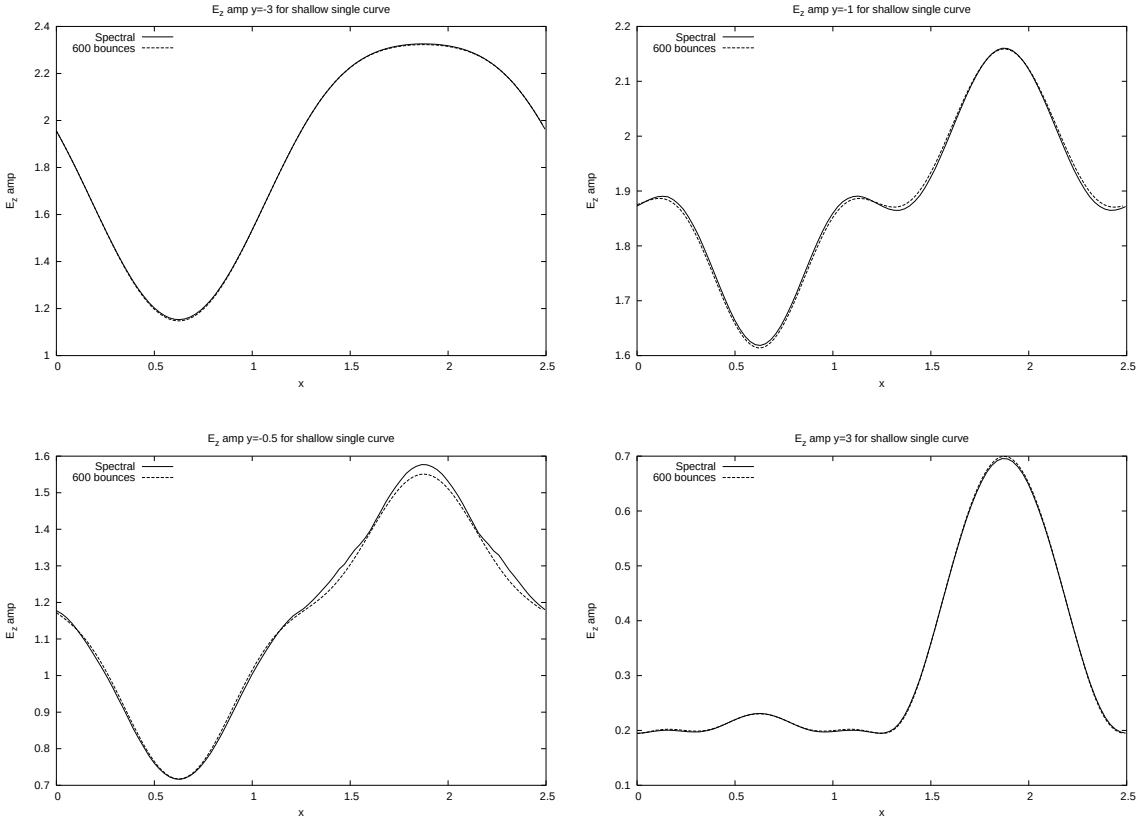

Fig. 7. E_z computed at different heights, y, with $y = 0$ corresponding to the vertical position of the shallow curved interface. Illumination is TE-polarized at normal incidence. Results are shown for converged solutions in terms of internal reflections and compared to a highly accurate spectral solution.

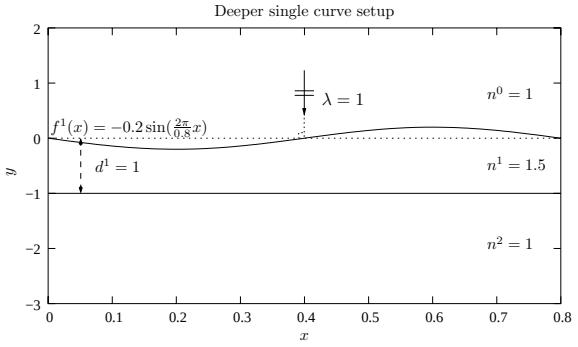

Fig. 8. Problem specification for a single layer with a deep curved interface.

w_ϵ	e_0^+	e_1^+	e_2^+	e_0^-	e_1^-	e_2^-	Total Efficiency - 1
10^{-3}	0.0175	0.0443	0.0032	0.7082	0.0814	0.0018	-1.30×10^{-03}
10^{-5}	0.0167	0.0458	0.0057	0.7108	0.0828	0.0019	-5.34×10^{-05}
10^{-7}	0.0167	0.0458	0.0057	0.7110	0.0828	0.0019	4.84×10^{-06}
10^{-9}	0.0167	0.0458	0.0057	0.7110	0.0828	0.0019	-1.64×10^{-08}
10^{-11}	0.0167	0.0458	0.0057	0.7110	0.0828	0.0019	-2.98×10^{-10}
10^{-13}	0.0167	0.0458	0.0057	0.7110	0.0828	0.0019	3.81×10^{-12}
10^{-15}	0.0167	0.0458	0.0057	0.7110	0.0828	0.0019	-1.54×10^{-14}
10^{-17}	0.0167	0.0458	0.0057	0.7110	0.0828	0.0019	-2.22×10^{-16}
10^{-19}	0.0167	0.0458	0.0057	0.7110	0.0828	0.0019	6.66×10^{-16}

Table 1. Convergence of scattering efficiencies and relation to threshold value, w_ϵ, used in iterative approach.

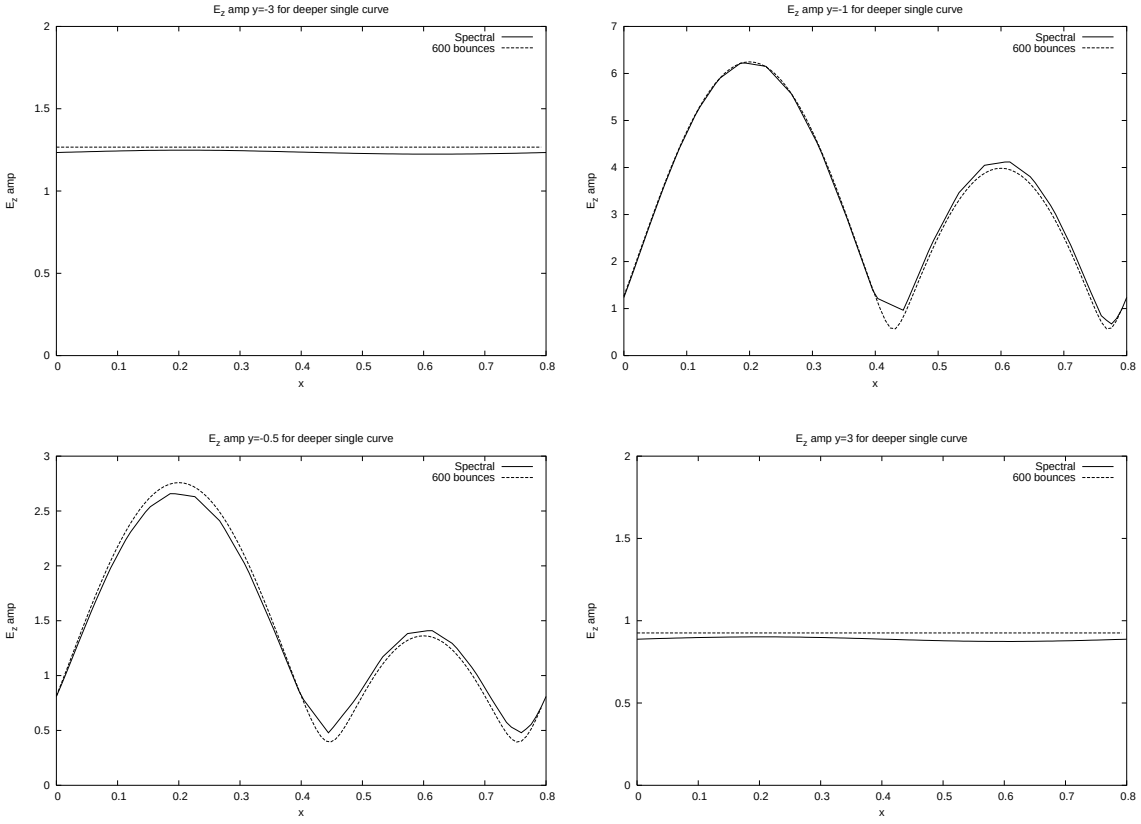

Fig. 9. E_z computed at different heights, y, with $y = 0$ corresponding to the vertical position of the deep curved interface. Illumination is TE-polarized at normal incidence. Results are shown for converged solutions in terms of internal reflections and compared to a highly accurate spectral solution.

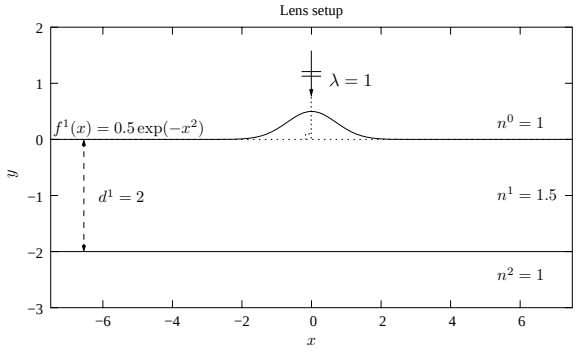

Fig. 10. Problem specification for a single layer with an integrated lens.

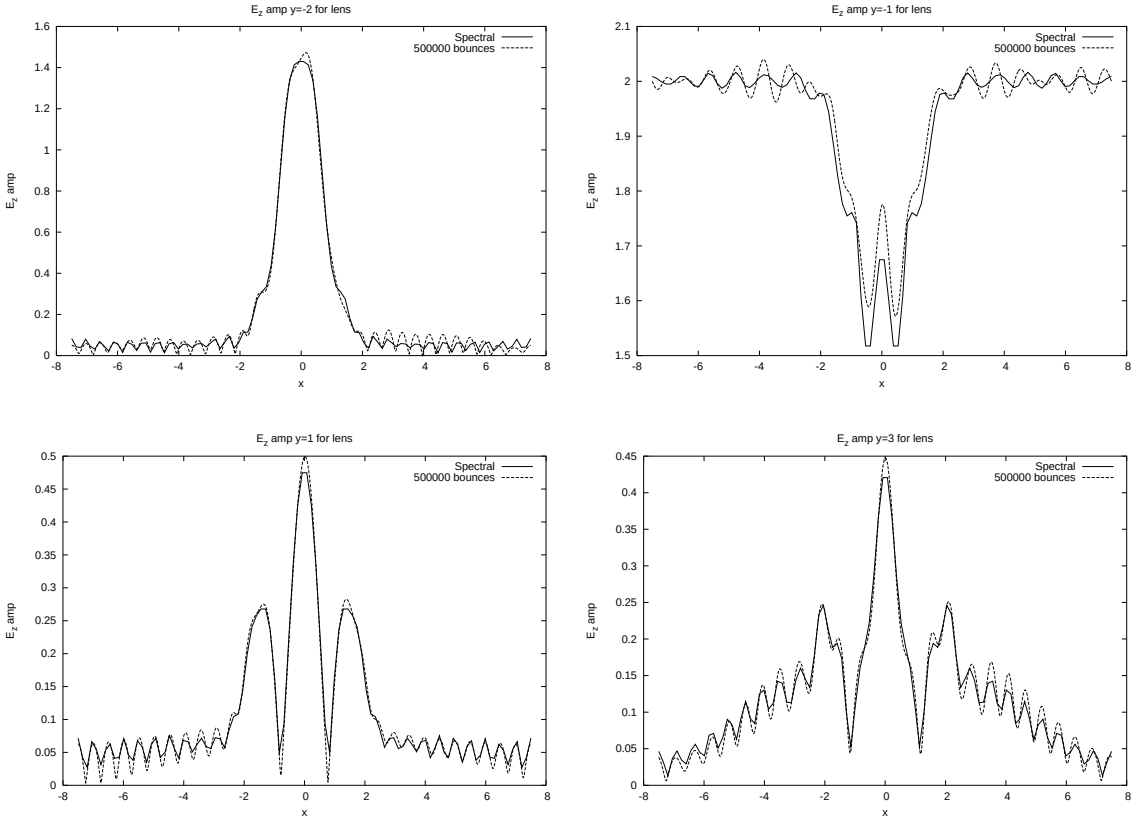

Fig. 11. E_z computed at different heights, y, with $y = 0$ corresponding to the vertical position of the integrated lens. Illumination is TE-polarized at normal incidence. Results are shown for converged solutions in terms of internal reflections and compared to a highly accurate spectral solution.

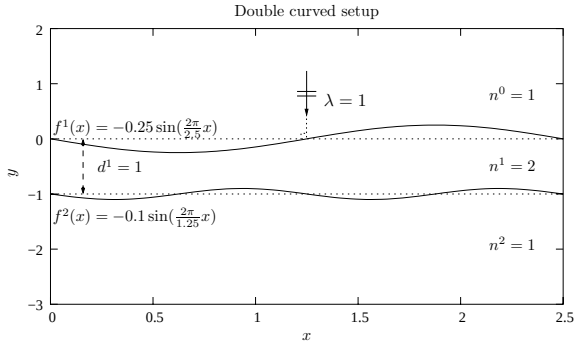

Fig. 12. Problem specification for a single layer with two curved interfaces.

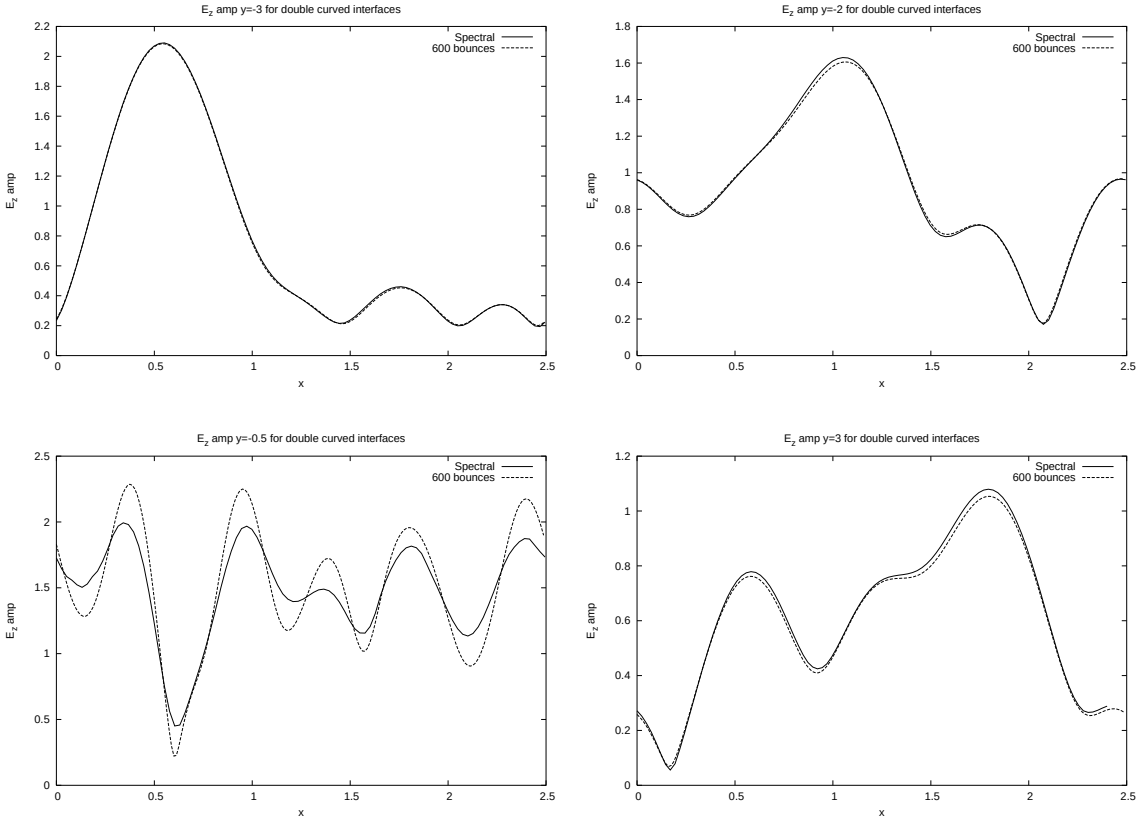

Fig. 13. E_z computed at different heights, y, with $y = 0$ corresponding to the vertical position of the slowly varying interface. Illumination is TE-polarized at normal incidence. Results are shown for converged solutions in terms of internal reflections and compared to a highly accurate spectral solution.